European Journal of Chemistry

Journal webpage: www.eurjchem.com

Density functional computational and X-ray studies on pharmaceutical compound 1-{3-[4-(4-fluorophenyl)piperazin-1-yl]propyl}-1*H*-indole

Zarife Sibel Şahin [1,*], Mine Yarım [2] and Meriç Köksal [2]

[1] *Sinop University, Faculty of Engineering and Architectures, Department of Energy Systems Engineering, 57000, Sinop, Turkey*
[2] *Yeditepe University, Faculty of Pharmacy, Department of Pharmaceutical Chemistry, 34755, Kayışdağı, İstanbul, Turkey*

** Corresponding author at: Sinop University, Faculty of Engineering and Architectures, Department of Energy Systems Engineering, 57000, Sinop, Turkey. Tel.: +90.546.4077397. Fax: +90.368.2714152. E-mail address: zarifesibel@sinop.edu.tr (Z.S. Şahin).*

ARTICLE INFORMATION

DOI: 10.5155/eurjchem.8.1.1-7.1512

Received: 01 December 2016
Received in revised form: 22 December 2016
Accepted: 25 December 2016
Published online: 31 March 2017
Printed: 31 March 2017

KEYWORDS

Indole
Piperazine
DFT calculations
Crystal structure
Frontier molecular orbitals
Molecular electrostatic potential map

ABSTRACT

The crystal and molecular structure of 1-{3-[4-(4-fluorophenyl)piperazin-1-yl]propyl}-1*H*-indole (I) has been determined by single-crystal X-ray diffraction. Molecular geometry of compound I in the ground state has been calculated using the density functional method (DFT) with B3LYP/6-31G(d,p) basis set and compared with the experimental data. In addition, density functional calculations of the structure, molecular electrostatic potential map, frontier molecular orbitals, atomic charges, thermodynamic functions and global chemical reactivity descriptors of compound I were performed.

Cite this: *Eur. J. Chem.* **2017**, *8(1)*, 1-7

1. Introduction

The class of σ receptors is subdivided into at least two subtypes, termed as σ1 and σ2 receptors. To date, the σ1 receptor is pharmacologically well characterized because of the receptor sequence information and availability of selective σ1 ligands. The 223-amino acid σ1 receptor with two trans-membrane-spanning regions [1,2] has been purified and cloned from several species, including mouse, rat, guinea pig and human [3-7]. Ligands interacting with σ receptors are of interest for example as atypical antipsychotics [8,9], antidep-ressants [10], anti-cocaine agents [11-13], and antitumor agents [14-17]. Thus, selective σ1 and σ2 agonists and antagonists may be potentially useful drugs for treatment of several pathologic conditions such as psychiatric disorders, cocaine abuse, memory and learning disorders, dyskinesia and dystonic reactions induced by classical antipsychotic drugs, cancer and tumor diagnosis.

Many important physiochemical properties of the chemical systems can be predicted from first principles by various computational techniques [18]. With recent advances in computer hardware and software, it is possible to correctly describe the chemical properties of molecules by various computational techniques [19].

Density functional theory (DFT) has been very popular for calculations in theoretical modeling since the 1970s. In many cases the results of DFT calculations for solid-state systems agreed quite satisfactorily with experimental data. DFT predicts a great variety of molecular properties: molecular structures, vibrational frequencies, atomization energies, ionization energies, electric and magnetic properties, reaction paths, etc.

In order to investigate the molecular features involved in sigma (σ) receptors binding, a series of compounds based on indole scaffolds were already synthesized and discussed [20]. In spide of its importance, mentioned above, X-ray crystal-lography and theoretical calculations of the title compound have not been investigated so far. In this work, the crystal and molecular structure of 1-{3-[4-(4-fluorophenyl)piperazin-1-yl]propyl}-1*H*-indole (**I**), one of the those compounds, has been determined by single-crystal X-ray diffraction. Besides, density functional calculations of the structure: molecular electrostatic potential, thermodynamic functions, frontier molecular orbitals, atomic charges and global chemical reactivity descriptors have been performed at the B3LYP/6-31G(d,p) level of theory.

ISSN 2153-2249 (Print) / ISSN 2153-2257 (Online) © 2017 Atlanta Publishing House LLC - All rights reserved - Printed in the USA
http://dx.doi.org/10.5155/eurjchem.8.1.1-7.1512

Table 1. Crystal data and structure refinement for compound **I**.

Empirical formula	$C_{21}H_{24}FN_3$
Formula weight	337.43
Temperature/K	296
Crystal system	Monoclinic
Space group	$P2_1/c$
a/Å	17.6087(11)
b/Å	5.9840(2)
c/Å	21.6813(16)
α/°	90.00
β/°	126.496(4)
γ/°	90.00
Volume/Å^3	1836.56(19)
Z	4
ρ_{calc}g/cm^3	1.220
μ/mm^{-1}	0.080
F(000)	720.0
Crystal size/mm^3	0.640 × 0.480 × 0.260
Radiation	MoKα (λ = 0.71073)
2Θ range for data collection/°	2.88 to 52
Index ranges	$-21 \le h \le 21, -7 \le k \le 7, -23 \le l \le 26$
Reflections collected	12542
Independent reflections	3619 [R_{int} = 0.0425]
Data/restraints/parameters	3619/2/227
Goodness-of-fit on F^2	0.898
Final R indexes [I≥2σ (I)]	R_1 = 0.0447, wR_2 = 0.1004
Final R indexes [all data]	R_1 = 0.1072, wR_2 = 0.1182
Largest diff. peak/hole / e Å^{-3}	0.09/-0.10

2. Experimental

2.1. Synthesis of 1-{3-[4-(4-fluorophenyl)piperazin-1-yl] propyl}-1H-indole (I)

To a solution of 4-fluorophenyl piperazine (5 mmol) in 10 mL of acetone was added 7.5 mL of a 25% solution sodium hydroxide. 30 minutes later, 1-bromo-3-chloropropane (5.5 mmol) was added carefully to minimize its mixing with aqueous layer. The mixture was stirred slowly for 22 h with a magnetic stirrer. The organic phase was then separated and the solvent was removed under vacuum. A mixture of indole (2.5 mmol) and 87% *w:v* solution KOH (7.5 mmol) in DMSO (30 mL) was stirred at room temp. for 1 h. Reaction mixture was cooled in ice-water bath to 0 °C and 1-(3-Chloropropyl)-4-(4-fluorophenyl)piperazine in DMSO (10 mL) was added dropwise. The stirring was continued at room temperature for 20-30 h. After addition of water (50 mL) and extraction with Et_2O, the organic layer was washed with water and dried over anhydrous Na_2SO_4. The solvent was evaporated and the oily residue was purified by column chromatography (SiO_2, AcOEt : *n*-hexane, 1:2) to give 1-{3-[4-(substituted phenyl)piperazin-1-yl]propyl}-1*H*-indole as an oil. These data about the compound were published in elsewhere [20]. Color: Colorless. Yield: 18%. FT-IR (KBr, ν, cm^{-1}): 3022-2763 (C-H), 1245 (C=C). ^{1}H NMR (400 MHz, $CDCl_3$, δ, ppm): 6.86-7.64 (m, 10H, indole + phenyl), 4.24 (t, 2H, indole N-CH_2-CH_2-CH_2), 3.13 (t,4H, piperazine H3, H5), 2.57 (t, 4H, piperazine H2, H6), 2.33 (t, 2H, CH_2-CH_2-CH_2-N piperazine), 2.03 (q, 2H, CH_2-CH_2-CH_2). ^{13}C NMR (100 MHz, $CDCl_3$, δ, ppm): 158.79, 155.45, 148.62, 136.40, 129.31, 128.73, 121.57, 119.49, 117.70, 117.64, 116.01, 115.79, 110,43, 101.13 (aromatics), 55,13 (indoleN-CH_2-CH_2-CH_2), 55.14 (piperazine C3, C5), 49.65 (piperazine C2, C6), 43.95 (CH_2-CH_2-CH_2-N piperazine), 27,67 (CH_2-CH_2-CH_2). Anal. calcd. for $C_{21}H_{24}FN_3$: C, 74.75; H, 7.17; N, 12.45. Found: C, 74.71; H, 7.13; N, 12.46%.

2.2. Crystallography

Colorless single-crystal of compound **I** suitable for data collection were selected and performed on a STOE IPDS II diffractometer with graphite monochromated MoK_α radiation λ = 0.71073 Å. The structures were solved by direct-methods using SHELXS-97 [21] and refined by full-matrix least-squares methods on F^2 using SHELXL-97 [21] from within the WINGX [22,23] suite of software. The parameters for data collection and structure refinement of compound **I** are listed in Table 1. All non-hydrogen atoms were refined with anisotropic parameters. Hydrogen atoms bonded to carbon were placed in calculated positions (C–H = 0.93-0.97 Å) and treated using a riding model with U = 1.2 times the U value of the parent atom for CH and CH_2. Molecular diagrams were created using MERCURY [24]. Geometric calculations were performed with PLATON [25]. Details of hydrogen-bond dimensions are given in Table 1.

2.3. Theoretical methods

All theoretical computations were done by using Gaussian 03 software package [26] and Gauss-view visualization program [27]. The compound **I** was optimized by using DFT method [28,29]. The initial guess of the compound was first obtained from the X-ray coordinates. DFT calculations with a hybrid functional B3LYP (Becke's three parameter hybrid functional using the LYP correlation functional) at 6-31G(d,p) basis set using the Berny method [30,31] were performed. To investigate the reactive sites of the compound **I**, the molecular electrostatic potentials were calculated using the same method. Additionally, we carried out calculations in four kinds of solvent (water, benzene, ethanol, and chloroform) in order to evaluate the solvent effect to total energy, HOMO and LUMO energies, dipole moment and chemical reactivity descriptors of the title compound. The computations were done with the B3LYP/6-31G(d,p) level using PCM model.

3. Results and discussion

3.1. Description of the crystal structure

The molecular structure of compound **I** was determined by X-ray crystallography have been depicted in Figure 1. The compound crystallizes in the space group $P2_1/c$ with Z = 4 and. The molecule is not planar. The compound contains a phenyl ring, a piperazine ring and a indole ring. The phenyl and indole rings are approximately planar and the dihedral angle of between these planes is 1.47°. The respective maximum deviations from the least-squares planes being 0.0091(14) Å for atom C16 and 0.0012(13) Å for atom N1. The piperazine ring exhibits a puckered conformation, with puckering parameters [32] q_2 = 0.0817(22) Å, q_3 = -0.5393(24) Å, Q_T = 0.5457(24) Å, ϕ = 178.2(18)° and θ = -171.26(23)°, which indicates that the piperazine ring has a chair conformation.

Table 2. Selected bond lengths and angles (Å, °).

	Experimental (X-ray)	Theoretical (DFT/B3LYP)
***Bond lengths* (Å)**		
C1–C6	1.405(3)	1.424
C7–C8	1.344(3)	1.370
C7–C6	1.359(2)	1.435
N2–C12	1.418(3)	1.463
N2–C15	1.456(2)	1.463
N3–C14	1.450(2)	1.458
N3–C13	1.459(2)	1.467
N1–C1	1.376(2)	1.384
N1–C8	1.371(2)	1.385
N1–C9	1.454(2)	1.455
N2–C11	1.455(3)	1.465
N3–C16	1.408(2)	1.416
F1–C19	1.360(3)	1.352
***Bond angles* (°)**		
C9–C10–C11	113.3(2)	113.7
C16–N3–C14	117.4(2)	117.7

Table 3. Hydrogen-bond parameters (Å, °) *.

D–H···A	D–H	H···A	D···A	D–H···A
C7-H7···Cg4 ^{i}	0.93	3.0366	3.836 (2)	144.98
C13-H13B···Cg3 ^{ii}	0.98	2.9845	3.910 (2)	159.87

* Symmetry codes: (i) -1/2+*x*, 1/2-*y*, -*z*; (ii) ½+*x*, 3/2-*y*, ½+*z*; Cg3: C1–C6 ring Cg4: C16–C21 ring.

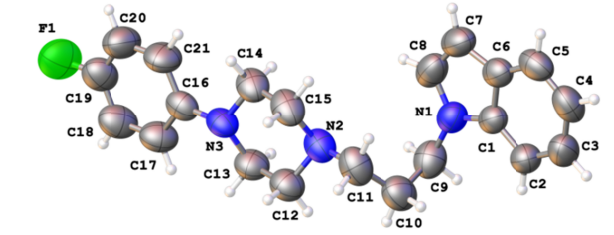

Experimental (X-ray)

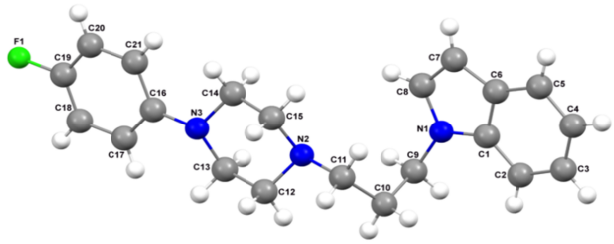

Theoretical (DFT/B3LYP)

Figure 1. The molecule of compound **I** showing the atom labeling scheme.

The selected bond lengths, bond angles and torsion angles are given in Table 2. The C19–F1 bond length is 1.360(3) Å, similar to the corresponding bond lengths [33]. The C–N bond distances in the piperazine and indole rings (Table 2) are as the expected single bond lengths, as reported in other piperazine and indole derivatives [34,35].

Molecules of compound **I** are linked to a three-dimensional framework by C–H···π interactions (Table 3). Atom C7 in the molecule at (x, y, z) acts as hydrogen-bond donor to the centroid Cg4^{i} ring, so forming a C(13) chain [36] running parallel to the [101] direction. Similarly, atom C13 serves as hydrogen-bond donor to the centroid Cg3^{ii} ring, so forming a C(10) chain running parallel to the [101] direction. The combination of the C(13) and C(10) chains generates a chain of edge-fused $R_4^4(32)$ rings (Figure 2).

3.2. Optimized geometry

The geometric parameters of I were calculated at the B3LYP/6-31G(d,p) level by DFT method and listed in Table 2, together with corresponding experimental values. As can be seen in Table 2, the bond lengths are extremely close to the experimental values. The biggest deviation of the selected bond lengths is 0.078 Å for C7–C6 bond. Furthermore, superimposition of the X-ray structure of the compound **I** (black) and its DFT (red) optimized counterpart, giving a RMSE of 0.332 Å was given in Figure 3. According to this result, it may be concluded that the B3LYP calculations well reproduce the geometry of compound **I**. The small differences between the calculated and observed geometrical parameters can be attributed to the fact that the theoretical calculations were carried out with isolated molecules in the gaseous phase whereas the experimental values were based on molecules in the crystalline state.

3.3. Frontier molecular orbitals (FMOs), total energies and chemical reactivity in solvent media

The lowest unoccupied molecular orbital (LUMO) and the highest occupied molecular orbital (HOMO) are often of particular interest as these are the orbitals most commonly involved in chemical reactions [37].

Table 4. Calculated energies, dipole moments, frontier orbital energies and chemical reactivity descriptors.

	Gas phase (ε=1)	Benzene (ε=2.3)	Chloroform (ε=4.9)	Ethanol (ε=24.55)
E_{total} (Hartree)	-1078.8025	-1078.8081	-1078.8122	-1078.8161
E_{HOMO} (eV)	-0.19486	-0.19561	-0.19659	-0.19746
E_{LUMO} (eV)	-0.00883	-0.00737	-0.00695	-0.00727
ΔE (eV)	0.18603	0.18824	0.18964	0.19019
D (Debye)	1.9892	2.2604	2.4462	2.6268
η (eV)	0.09302	0.09412	0.09482	0.09510
S (eV^{-1})	10.7504	10.6247	10.5463	10.5158
μ (eV)	-0.10183	-0.10149	-0.10177	-0.10237
χ (eV)	0.10183	0.10149	0.10177	0.10237
ω (eV)	0.05576	0.05472	0.05461	0.05594

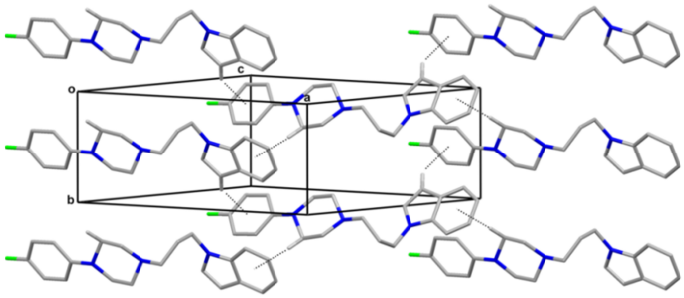

Figure 2. Crystal structure of compound **I**, showing the formation of a $R_4^2(32)$ rings.

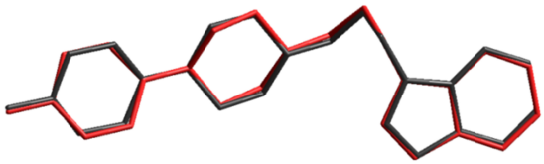

Figure 3. Atom-by-atom superimposition of the calculated structure (red) over the X-ray structure (black) for the title compound.

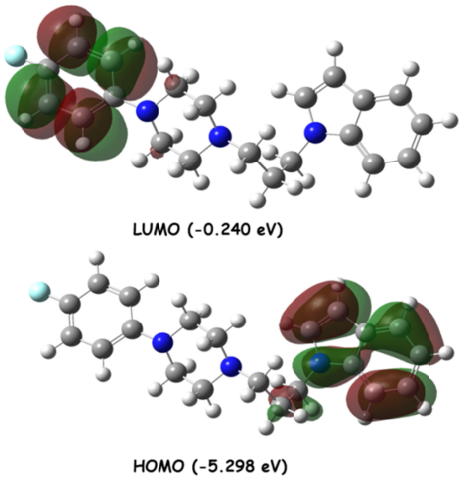

Figure 4. Molecular orbital surfaces and energy levels for the HOMO and LUMO of the title compound computed at B3LYP/6-31G(d,p) level.

The HOMO and LUMO are also important in determining such properties as molecular reactivity and the ability of a molecule to absorb light. Figure 4 shows the distributions and energy levels of the HOMO and LUMO orbitals computed at the B3LYP/6-31G(d,p) level for compound **I**. As can be seen in Figure 4, the HOMOs are mainly localized on the around indole ring where the LUMOs are populated on the phenyl ring.

We carried out calculations in three kinds of solvent (benzene, ethanol, chloroform) in order to evaluate the solvent effect to the total energy, HOMO and LUMO energies, dipole moment and chemical reactivity descriptors of the title compound. The computations were done with the B3LYP/6-31G(d,p) level using PCM model and the results are given in Table 4.

Table 5. Calculated net charges by Mulliken population method.

Atom	Mulliken charges	Atom	Mulliken charges
C1	0.370407	C14	-0.020510
C2	-0.141493	C15	-0.022341
C3	-0.085580	C16	0.338599
C4	-0.101664	C17	-0.088027
C5	-0.097919	C18	-0.096745
C6	0.280416	C19	0.326612
C7	-0.080853	C20	-0.096125
C8	0.580953	C21	-0.090987
C9	-0.023377	F1	-0.314963
C10	-0.192327	N1	-0.550398
C11	-0.011916	N2	-0.480526
C12	-0.025349	N3	-0.575855
C13	-0.021697		

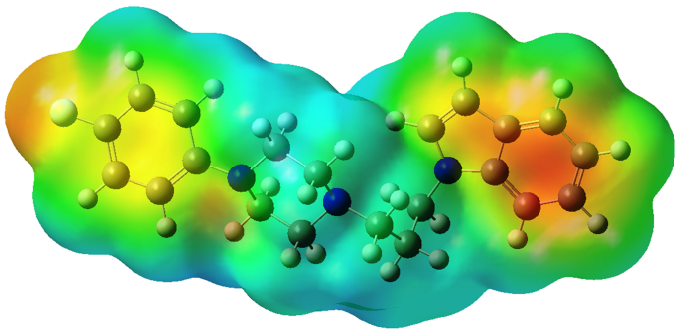

Figure 5. Molecular electrostatic potential map of compound **I** calculated at DFT/B3LYP/6-31G(d, p) level.

The electronic chemical potential μ is given as the first derivative of the energy with respect to the number of electrons, which in a finite difference version is given as the average of the ionization potential (IP) and electron affinity (EA). Except for a difference in sign, this is also the Mulliken definition of electronegativity χ [38].

$$-\mu = \chi = \frac{\delta E}{\delta N_{elec}} = \frac{1}{2}(IP + EA) \quad (1)$$

The second derivative of the energy with respect to the number of electrons is hardness η (the inverse quantity η^{-1} is called the softness (S)), which again may be approximated in term of the ionization potential and electron affinity [38].

$$\eta = \frac{1}{2}\frac{\delta^2 E}{\delta N_{elec}^2} = \frac{1}{2}(IP - EA) \quad (2)$$

The electrophilicity, which measures the total ability to attract electrons, is defined as following

$$\omega = \frac{\mu^2}{2\eta} = \frac{(IP+EA)^2}{4(IP-EA)} \quad (3)$$

These concepts play an important role in the hardness and softness of molecules. A hard molecule has a large HOMO-LUMO gap, and a large HOMO-LUMO gap implies high kinetic stability and low chemical reactivity, as it is energetically unfavorable to add electron to a high-lying LUMO, to extract electrons from low-lying HOMO [39]. Polarizability is also related to the HOMO-LUMO gap. A small HOMO-LUMO gap indicates a soft molecule and a small energy gap will give a large contribution to the polarizability. Softness is a measure of how easily the electron density can be distorted by external fields [38].

As can been seen in Table 4, we can conclude that the HOMO-LUMO energy gaps, the hardness, dipole moment and the stability of the molecule increase with the increasing polarity of the solvent.

3.4. Molecular electrostatic potential

Molecular electrostatic potential (MEP) maps are often used for the qualitative interpretation of electrophilic and nucleophilic reactions [40], rationalize intermolecular interact-tions between polar species, the calculation of atomic charges [41] and define regions of local negative and positive potential in the molecule [42]. This surface represents the distance from a molecule at which a positive test charge experiences a certain amount of attraction or repulsion. To investigate the reactive sites of **I** the molecular electrostatic potentials were evaluated using the B3LYP/6-31G(d,p) method. The negative (red) regions of MEP were related to electrophilic reactivity and the positive (blue) regions to nucleophilic reactivity. The electrostatic potential *V(r)* is also well suited for analyzing processes based on the "recognition" of one molecule by another, as in drug-receptor, and enzyme-substrate interactions, because it is through their potentials that the two species first "see" each other [43-45]. As it can be seen in Figure 5, the red regions are chiefly concentrated on the indole and phenyl rings. According to these results, the phenyl and indole rings are the most suitable regions for the electrophilic reaction and they can easily react with atoms having high electrophilic attraction such as metal atoms.

3.5. Mulliken population analysis

In addition to molecular electrostatic potential analysis, Mülliken population analysis play an important role in the determination of molecular polarizability, electronic structure, acidity-basicity behavior and a lot of properties of molecular system. The Mülliken atomic charges of the title compound are listed in Table 5 and graphically shown in Figure 6. It is seen that all nitrogen atoms and fluorine atom have negative charge. The N3 atom (-0.575855) has the most negative charges, while the C8 (0.580953) atom has the most positive charges.

Table 6. Thermodynamic properties of the title compound at different temperatures.

Temperature (K)	100	200	300	400	500
H (kcal/mol)	2.0996	6.4446	13.4229	23.2463	35.7065
C (cal/mol·K)	29.8331	56.0084	82.1173	110.123	134.508
S (cal/mol.K)	94.9174	124.066	151.973	180.044	204.741
$E_{Thermal}$(kcal/mol)	253.384	257.536	264.322	273.955	286.223

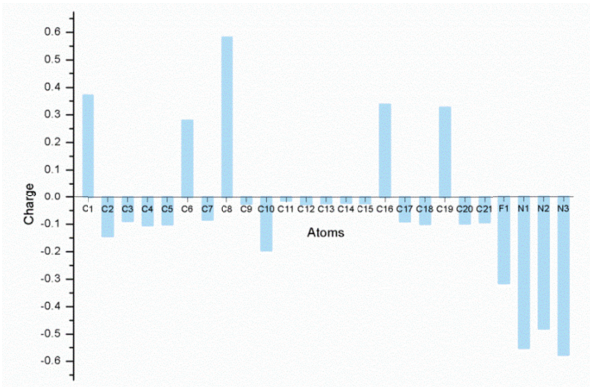

Figure 6. Calculated net charges by Mulliken population method plots for the title compound (Hydrogen atoms are omitted for clarity).

3.6. Thermodynamic properties

Thermodynamic properties are the key in the understanding and design of chemical processes. DFT calculations also enable predictions to be made of the thermodynamic properties of systems for which there is no experimental data, or for which experimental data is difficult or impossible to obtain [37].

The entropy (S) and heat capacity (C) are calculated as the following [46-48]

$$S = S_{trans} + S_{rot} + S_{vib} \quad (4)$$

$$= R\left[\frac{3}{2}\ln\left(\frac{2\pi mkT}{h^2}\right) + ln\frac{kT}{p} + \frac{5}{2}\right] + R\left[ln\frac{\sqrt{\pi}}{\sigma_T} + \frac{1}{2}ln\frac{T^3}{(h^2/8\pi^2 I_x k)(h^2/8\pi^2 I_y k)(\frac{h^2}{8\pi^2 I_z k})} + \frac{3}{2}\right] + R\left[\sum_{i=1}^{3N-6}\left[\frac{h\nu/kT}{\exp(\frac{h\nu}{kT})-1} - \ln(\exp(-h\nu/kT))\right]\right] \quad (5)$$

$$C = C_{trans} + C_{rot} + C_{vib} = \frac{5}{2}R + \frac{3}{2}R + R\sum_{i=1}^{3N-6} exp\left(\frac{h\nu}{kT}\right)\left[\frac{h\nu/kT}{\exp(\frac{h\nu}{kT})-1}\right] \quad (6)$$

where $S_{trans}, S_{rot}, S_{vib}$ and $C_{trans}, C_{rot}, C_{vib}$ are translational, rotational and vibrational entropy and heat capacity, respectively. R is the gas constant (8.31451 J/mol·K), N is the atom number in a molecule, m is the molecular mass, k is the Boltzmann constant (1.380658×10^{-23} J/K), h is the Planck's constant (6.6260755×10^{-34} J.s), T is the temperature, p is the pressure, σ_T is the symmetry number for rotation, I is the moment of inertia and ν is the vibrational frequency.

The absolute internal energy (U), enthalpy (H) and Gibbs energy (G) of the molecule are calculated as following at 0 K and the specified temperature (T) [46-48]

$$U_{0K} = E_{elec} + E_{ZPE} \quad (7)$$

$$U_T = U_{0K} + (E_{trans} + E_{rot} + E_{vib})_T \quad (8)$$

$$H_T = U_T + RT \quad (9)$$

$$G_T = H_T - TS \quad (10)$$

where E_{elec} is the internal energy due to electronic motion and E_{ZPE} is the zero point energy of the molecule at 0 K. E_{trans}, E_{rot} and E_{vib} are the thermal energy corrections due to the effects of molecular translation, rotation and vibration at the specified temperature, respectively.

On the basis of theoretical harmonic frequencies obtained from density functional calculations at B3LYP/6-31G(d,p) level, the statistical standard thermodynamic functions, viz., heat capacities (C), entropies (S) and enthalpy (H) ($100 \le T/K \le 500$) for the title compound were obtained and listed Table 6. In the calculations, the ideal gas approximation and non-interacting particles of the reaction systems are assumed. The scaling factor for the vibrational frequencies is also 0.9627 [49,50], which is used for an accurate prediction in determining the thermodynamic functions.

As seen in Table 6, we can see that the standard heat capacities, entropies and enthalpy changes are increasing with temperatures ranging from 100 to 500 K due to the fact that the molecular vibrational intensities are increasing with temperatures. As the temperature increases, the entropy of the atoms in the lattice increases. Vibrational motions cause the atoms and molecules in the lattice to be less well ordered.

The correlation equations between thermodynamic properties $C^o_{p,m}$, S^o_m and H^o_m and temperatures were fitted by quadratic formulas and the corresponding fitting factors (R^2) for these thermodynamic properties are all beyond 0.999. The correlation equations of the title compound are as follows:

$$H = 0.54098+0.00233T+1.4156\times10^{-4}T^2 \quad r^2 = 0.9999 \quad (11)$$

$$C = 2.739+0.25463T+4.5207\times10^{-5}T^2 \quad r^2 = 0.9879 \quad (12)$$

$$S = 68.4434+0.30474T-2.0342\times10^{-6}T^2 \quad r^2 = 0.9999 \quad (13)$$

The results can be used to calculate thermodynamic parameters for unknown data in further studies. They can be used to compute the other thermodynamic energies according to relationships of thermodynamic functions and be beneficial to synthesize similar molecules in further studies.

4. Conclusions

In this study, the crystal and molecular structure of 1-{3-[4-(4-fluorophenyl)piperazin-1-yl]propyl}-1*H*-indole (**I**) has

been determined by single-crystal X-ray diffraction. Molecules of compound **I** are linked to a three-dimensional framework by C–H···π interactions. Molecular geometry of compound **I** in the ground state has been calculated using the density functional method (DFT) with B3LYP/6-31G(d,p) basis set and compared with the experimental data. Despite the differences observed in the geometric parameters, the general agreement is good and theoretical calculations support the solid-state structure. In addition, HOMO and LUMO orbitals computed at the B3LYP/6-31G(d,p) level for compound **I**. It is seen that the HOMOs are mainly localized on the around indole ring where the LUMOs are populated on the phenyl ring. We carried out calculations in three kinds of solvent (benzene, ethanol, chloroform) in order to evaluate the solvent effect to the total energy, HOMO and LUMO energies, dipole moment and chemical reactivity descriptors of the title compound and it is seen that the HOMO-LUMO energy gaps, the hardness, dipole moment and the stability of the molecule increase with the increasing polarity of the solvent. According to MEP map of the molecule, the phenyl and indole rings are the most suitable regions for the electrophilic reaction and they can easily react with atoms having high electrophilic attraction such as metal atoms. Besides, on the basis of theoretical harmonic frequencies obtained from density functional calculations at B3LYP/6-31G(d,p) level, the statistical standard thermos-dynamic functions, viz., heat capacities (*C*), entropies (*S*) and enthalpy (*H*) ($100 \leq T/K \leq 500$) for the title compound were obtained and it is seen that the standard heat capacities, entropies and enthalpy changes are increasing with temperatures ranging from 100 to 500 K due to the fact that the molecular vibrational intensities are increasing with temperatures. We hope the results of this study will help researchers to design and synthesis new materials.

Acknowledgement

We sincerely thank to Professor Şamil Işık for his help with the data collection.

Supplementary data

Crystallographic data for the structure reported in this article have been deposited with the Cambridge Crystallographic Data Centre as supplementary publication number 1037165. Copies of the data can be obtained free of charge on application to CCDC 12 Union Road, Cambridge CB21 EZ, UK. (Fax: (+44) 1223 336 033; e-mail: data_request@ccdc.cam.ac.uk).

References

[1]. Aydar, E.; Palmer, C. P.; Klyachko, V. A.; Jackson, M. B. *Neuron* **2002**, *34*, 399-410.
[2]. Jbilo, O.; Vidal, H.; Paul, R.; Nys, N. D.; Bensaid, M.; Silve, S.; Carayon, P.; Davi, D.; Galiegue, S.; Bourrie, B.; Guillemot, J. C.; Ferrara, P.; Loison, G.; Maffrand, J. P.; Le Fur, G.; Casellas, P. *J. Biol. Chem*. **1997**, *272,* 27107-27115.
[3]. Hanner, M.; Moebius, F. F.; Flandorfer, A. A.; Knaus, H. G.; Striessnig, J.; Kempner, E.; Glossmann, H. *Proc. Natl. Acad. Sci. USA* **1996**, *93*, 8072-8077.
[4]. Mei, J. F.; Pasternak, G. W. *Biochem. Pharmacol* **2001**, *62*, 349-355.
[5]. Pan, Y. X.; Mei, J.; Xu, J.; Wan, B. L.; Zuckerman, A.; Pasternak, G. W. *J. Neurochem.* **1998**, *70,* 2279-2285.
[6]. Seth, P.; Leibach, F. H.; Ganapathy, V. *Biochem. Biophys. Res. Commun* **1997**, *241*, 535-540.
[7]. Seth, P.; Fei, Y. J.; Li, H. W.; Huang, W.; Leibach, F. H.; Ganapathy, V. *J. Neurochem.* **1998**, *70,* 922-931.
[8]. Abou-Gharbia, M.; Ablordeppey, S. Y.; Glennon, R. *Ann Rep Med Chem*. **1993**, *28,* 1-10.
[9]. Hayashi, T.; Su, T. P. *CNS Drugs* **2004**, *18*, 269-284.
[10]. Sorbera, L. A.; Silvestre, J.; Castaner, J. *Drugs Fut*. **1999**, *24*, 133-140.
[11]. Foster, A.; Wu, H.; Chen, W.; Williams, W.; Bowen, W. D.; Matsumoto, R. R. *A. Coop, Bioorg. Med. Chem. Lett*. **2003**, *13*, 749-751.
[12]. Matsumoto, R. R.; Liu, Y.; Lerner, M.; Howard, E. W.; Bracket, D. J. *Eur. J. Pharmacol*. **2003**, *469*, 1-12.
[13]. Matsumoto, R. R.; McCracken, K. A.; Pouw, B.; Miller, J.; Bowen, W. D.; Williams, W.; deCosta, B. R. *Eur. J. Pharmacol*. **2001**, *411,* 261-273.
[14]. Crawford, K. W.; Bowen, W. D. *Cancer Res*. **2002**, *62*, 313-322.
[15]. Spruce, B. A.; Campbell, L. A.; McTavish, N.; Cooper, M. A.; Appleyard, V. L.; O'Neill, M.; Howie, J.; Samson, J.; Watt, S.; Murray, K.; McLean, D.; Leslie, N. R.; Safrany, S. T.; Ferguson, M. R.; Peters, J. A.; Prescott, A. R.; Box, G.; Hayes, A.; Nutley, B.; Raynaud, F.; Downes, C. P.; Lambert, J. J.; Thompson, A. M.; Eccles, S. *Cancer Res*. **2004**, *64*, 4875-4886.
[16]. Choi, S. R.; Yang, B.; Plossl, K.; Chumpradit, S.; Wey, S. P.; Acton, P. D.; Wheeler, K.; Mach, R. H.; Kung H. F. *Nucl. Med. Biol.* **2001**, *28,* 657-666.
[17]. John, C. S.; Lim, B. B.; Vilner, B. J.; Geyer, B. C.; Bowen, W. D. *J. Med. Chem.* **1998**, *41,* 2445-2450.
[18]. Lipkowitz, K. B.; Boyd, D. Reviews in Computational Chemistry, Eds.; VCH: New York, Vols. 1-13, 1990-1999.
[19]. Zhang, Y.; Guo, A. J.; You, X. Z. *J Am Chem Soc.* **2001**, *123,* 9378-9387.
[20]. Yarim, M.; Koksal, M.; Schepmann, D.; Wünsch, B. *Chem Biol Drug Des.* **2011**, *78(5)*, 869-875.
[21]. Sheldrick, G. M. *Acta Cryst. A* **2008**, *64,* 112-122.
[22]. Farrugia, L. J. WINGX-A Windows Program for Crystal Structure Analysis, University of Glasgow, 1998.
[23]. Farrugia, L. J. *J. Appl Crystallogr*. **1999**, *30*, 837-838.
[24]. Mercury, version 3. 0; CCDC, available online via ccdc. cam. ac. uk/products/mercury.
[25]. Spek, A. L. PLATON-A Multipurpose Crystallographic Tool, Utrecht, Utrecht University, The Netherlands, 2005.
[26]. Frisch, M. J.; Trucks, G. W.; Schlegel, H. B.; Scuseria, G. E.; Robb, M. A.; Cheeseman, J. R.; Jr. Montgomery, J. A.; Vreven, J. T.; Kudin, K. N.; Burant, J. C.; Millam, J. M.; Iyengar, S. S.; Tomasi, J.; Barone, V.; Mennucci, B.; Cossi, M.; Scalmani, G.; Rega, N.; Petersson, G. A.; Nakatsuji, H.; Hada, M.; Ehara, M.; Toyota, K.; Fukuda, R.; Hasegawa, J.; Ishida, M.; Nakajima T.; Honda, Y.; Kitao, O.; Nakai, H.; Klene, M.; Li, X.; Knox, J. E.; Hratchian, H. P.; Cross, J. B.; Bakken, V.; Adamo, C.; Jaramillo, J.; Gomperts, R.; Stratmann, R. E.; Yazyev, O.; Austin, A. J.; Cammi, R.; Pomelli, C.; Ochterski J. W.; Ayala P. Y.; Morokuma, K.; Voth, G. A.; Salvador, P.; Dannenberg, J. J.; Zakrzewski, V. G.; Dapprich, S.; Daniels, A. D.; Strain, M. C.; Farkas, O.; Malick, D. K.; Rabuck, A. D.; Raghavachari, K.; Foresman, J. B.; Ortiz, J. V.; Cui, Q.; Baboul, A. G.; Clifford, S.; Cioslowski, J.; Stefanov, B. B.; Lui, G.; Liashenko, A.; Piskorz, P.; Komaromi, I.; Martin, R. L.; Fox, D. J.; Keith, T.; Al-Laham, M. A.; Peng, C. Y.; Nanayakkara, A.; Challacombe, M.; Gill, P. M. W. B.; Johnson, B.; Chen, W.; Wong, M. W.; Gonzalez, C.; Pople, J. A. GAUSSIAN 03, Revision C. 02, Gaussian Inc, Wallingford CT. , 2004.
[27]. Frisch, A.; Dennington II, R. D.; Keith, T. A.; Milliam, J.; Nielsen, A. B.; Holder, A. J.; Hiscocks, J. GaussView Reference, Version 4. 0. Gaussian Inc. , Pittsburgh, 2007.
[28]. Hohenberg, P.; Kohn, W. *Phys. Rev. B* **1964**, *136*, 846-864.
[29]. Kohn, W.; Sham, L. J. *Phys. Rev. A* **1965**, *140*, 1133-1138.
[30]. Peng, C.; Ayala, P. Y.; Schlegel, H. B.; Frisch, M. J. *J Comput Chem*. **1996**, *17*, 43-49.
[31]. Stephens, P. J.; Devlin, F. J.; Chablowski, C. F.; Frisch, M. J. *J Phys Chem*. **1994**, *98*, 11623-11627.
[32]. Cremer, D.; Pople, J. A. *J. Am. Chem. Soc.* **1975**, *97,* 1354-1358.
[33]. Sahin, Z. S.; Isık, S.; Salgın-Goksen, U.; Gokhan-Kelekci, N. *Chinese J. Struct. Chem.* **2010**, *29,* 700-705.
[34]. Sahin, Z. S.; Ozkan, I.; Koksal, M.; Isık, S. *J. Struct. Chem*. **2012**, *53,* 938-941.
[35]. Li, Y.; Sun, H.; Jiang, H.; Xu, N.; Xu, H. *Acta Cryst. E* **2014**, *70,* 259-261.
[36]. Bernstein, J.; Davis, R. E.; Shimoni, L.; Chang, N. L. *Angew. Chem. Int. Ed. Engl.* **1995**, *34,* 1555-1573.
[37]. Leach, A. R. Molecular modelling-Principles and applications, Prentice Hall, 2nd edn, Harlow, 2001.
[38]. Jensen, F. Introduction to computational chemistry, Wiley: 2nd ed. Chichester, UK, 2006.
[39]. Aihara, J. *J. Phys. Chem. A* **1999**, *103,* 7487-7495.
[40]. Politzer, P.; Daiker, K. C. Models for Chemical Reactivity. In The Force Concept in Chemisty Van Nostrand Reinhold New York, 1981.
[41]. Cox, S. R.; Williams, D. E. *J. Compt. Chem.* **1981**, *2,* 304-323.
[42]. Carbo, R.; Calabuig, B. *Compt. Phys. Commun*. **1989**, *55,* 117-126.
[43]. Politzer, P.; Truhlar, D. G. In: Chemical Applications of Atomic and Molecular Electrostatic Potentials Plenum, New York, 1981.
[44]. Scrocco, E.; Tomasi, J. *Top. Curr. Chem*. **1973**, *42,* 69-95.
[45]. Sahin, Z. S.; Salgin-Goksen, U.; Gokhan-Kelekci, N.; Isik, S. *J. Mol. Struct*. **2011**, *1006*, 147-158.
[46]. McQuarrie, D. A. *Molecular Thermodynamics*, Calif. , University Science Books, Sausalito, 1999.
[47]. Hehre, W. J. *AB initio Molecular Orbital Theory*, Wiley: New York, 1986.
[48]. Li, X. W.; Shibata, E.; Nakamura, T. *Materials Trans.* **2003**, *44-5*, 1004-1007.
[49]. Merrick, J. P.; Moran, D.; Radom, L. *J. Phys. Chem. A* **2007**, *111,* 11683-11700.
[50]. Sahin, Z. S.; Kaya-Kantar, G.; Sasmaz, S.; Buyukgungor, O. *J. Mol. Struct*. **2015**, 1087, 104-112.